

A Physical Model of Time-of-Flight 3D Imaging Systems, Including Suppression of Ambient Light

Mirko Schmidt and Bernd Jähne

Heidelberg Collaboratory for Image Processing (HCI),
Interdisciplinary Center for Scientific Computing (IWR),
University of Heidelberg,
69115 Heidelberg, Germany
{mirko.schmidt,bernd.jaehne}@iwr.uni-heidelberg.de

Abstract. We have developed a physical model of continuous-wave Time-of-Flight cameras, which focuses on a realistic reproduction of the sensor data. The derived simulation gives the ability to simulate data acquired by a ToF system with low computational effort. The model is able to use an arbitrary optical excitation and to simulate the sampling of a target response by a two-tap sensor, which can use any switching function. Nonlinear photo response and pixel saturation, as well as spatial variations from pixel to pixel like *photo response non-uniformity* (PRNU) and *dark signal non-uniformity* (DSNU) can be modeled. Also the influence of interfering background light and on-sensor suppression of ambient light can be simulated.

The model was verified by analyzing two scenarios: The cameras response to an increasing, homogeneous irradiation as well as the systematic phase deviation caused by higher harmonics of the optical excitation. In both scenarios the model gave a precise reproduction of the observed data.

1 Introduction

Time-of-flight (ToF) 3-D cameras measure the distance of the object by determining the time τ_d which the light needs to cover the distance from a light source to the object and from the object to the sensor. With c being the speed of light, the distance d of the imaged point can be computed as

$$d = \frac{1}{2} \cdot c \cdot \tau_d, \quad (1)$$

where the light source is assumed to be located near the camera. ToF cameras measure this distance in each pixel - enabling the simultaneous generation of dense depth maps. Pulse-based and a phase-based ToF cameras have been realized.

The pulse based method employs discrete pulses of light which are emitted by a light source and backscattered by the object. In [3] a CMOS sensor was

presented, which can be shuttered electronically extremely fast and with a very high precision. Another method was used in [16]: Here a conventional 2D imaging sensor is combined with a physical shutter, which can be modulated in transmissivity. This physical shutter ensures that light reaches the sensor only in a certain time window, which enables the estimation of the objects distance from the detected intensity values.

With a continuous-wave, amplitude-modulated light source the depth is determined by measuring the phase-shift between the emitted and the received optical signal. For a periodical modulation of frequency ν , the phase shift φ corresponds to a temporal shift

$$\tau_d = \frac{\varphi}{2\pi\nu}, \quad (2)$$

which gives the distance by using (1):

$$d = \frac{\varphi}{4\pi\nu} \cdot c. \quad (3)$$

To measure the phase shift between the reflected optical signal and the electronic reference signal, special sensors called *Photonic Mixing Device* (PMD) were developed. They use pixel with two quantum wells to perform a correlation of both signals. In 1995 the first sensors using such a pixelwise on-chip correlation were presented in [14] and [15]. Currently the ToF camera systems of manufacturers like *PMDTec* [12], *Mesa Imaging* [8] and *Canesta* [4] are using this approach.

The correlation function of a sinusoidal electrooptical signal $S(t)$ with an electronic reference signal $R(t)$ delayed by a phase angle Θ , assuming an angular frequency ω and a correlation range of m oscillating periods, is given by

$$\begin{aligned} S(t) &= G_0 + A \sin(\omega t - \varphi), \\ R(t) &= H(\sin(\omega t + \Theta)), \\ I(\Theta) &= mT \left(\frac{A}{\pi} \cos(\varphi + \Theta) + \frac{G_0}{2} \right). \end{aligned}$$

H is the Heaviside step function, meaning that $R(t)$ is assumed to be rectangular. The rectangular shaped reference signal is a good approximation of a real PMD sensor reference signal, which results from a discrete switching of the electrical field inside the sensor. G_0 is a constant describing the offset of the light source, and A is its amplitude. The full derivation is available for instance in [13].

The PMD-Sensor is able to sample the correlation function at different phasings by electronically delaying the reference signal by angle Θ . Besides the objects distance, also the intensity of the light source and of a possible background illumination are unknown. Therefore at least three measurements are necessary to estimate them.

From N equidistant sampling points located at the phase angles Θ_n , the offset a_0 , amplitude a_1 and the phase shift φ of the electrooptical input signal may

be estimated. Most available ToF systems use $N = 4$ samples, but also systems using more or fewer samples are feasible. As shown e.g. by [10], the optimal solution in a least square sense is given by (4) - (6) and their variance may be estimated as shown in (7) - (9). This is derived by using Gaussian error propagation and assuming an equal variance σ^2 of all acquired raw intensity values I_n .

However, in practice this simplified assumption does not hold: It does not account for a variety of factors like

- non sinusoidal light modulation $S(t)$
- non rectangle switching function $R(t)$
- non-linear photo-response
- influence of on-sensor suppression of ambient light.

Furthermore spatial variations from pixel to pixel like *photo response non-uniformity* (PRNU), *dark signal non-uniformity* (DSNU), and *dark current non-uniformity* (DCNU) (see [2]) must be considered.

$$a_0 = \frac{2}{N} \sum_{n=0}^{N-1} I_n \quad (4) \quad \sigma_{a_0}^2 = \frac{\sigma^2}{4} \quad (7)$$

$$a_1 = \frac{2\pi}{N} \left| \sum_{n=0}^{N-1} I_n e^{-i2\pi(n/N)} \right| \quad (5) \quad \sigma_{a_1}^2 = \frac{\sigma^2}{2} \quad (8)$$

$$\varphi = \arg \left(\sum_{n=0}^{N-1} I_n e^{-i2\pi(n/N)} \right) \quad (6) \quad \sigma_{\varphi}^2 = \frac{\sigma^2}{2a_1^2} \quad (9)$$

$$\text{with } I_n = \frac{I(\Theta_n)}{mT}$$

1.1 Motivation and Related Work

To describe these effects, a detailed physical model of a ToF sensor is necessary, similar to that proposed by [2] for linear 2D-Sensors. With a thorough calibration this model could help improving current ToF systems.

Our goal is to simulate the data produced by a ToF camera as realistic as possible, so the optimization of existing ToF systems as well as the prediction of the characteristics of yet unavailable cameras gets feasible.

Prior models do not include all the effects discussed in the previous section. They rather focused on the simulation of whole 3D scenes. In [5] a MATLAB-based approach was chosen, where the resulting point cloud of a 3D scene is represented as superposition of single point responses. The influence of an area light source and inhomogeneous illumination of the scene was simulated by [9]. In [6,7] a simulation tool for real-time ToF data was presented. It uses the GPU to generate synthetic data for whole 3D scenes, which can be static or moving.

All these approaches focus on the simulation of ToF data for a given 3D scene. This includes issues of rendering, an adequate camera model, reflectance characteristics of the imaged objects and the position and size of the light sources. From the given ideal depth image the simulated samples are generated using a measured correlation function of a real PMD. A very simple noise model is employed to simulate the influence of noise on the acquired data. From the noisy samples, a depth image is computed.

In contrast this paper focuses on the effects influencing the quality of the generated depth image, and their origin. That means we concentrated on modeling the sensor and its noise sources very carefully. But we made only small efforts to simulate the imaging of the scene. In fact we use ideal depth maps and reflectivity maps as input for our model.

The structure of this paper is as follows: In section 2 the physical model of ToF cameras is presented, starting on a conceptual level and then explaining some necessary speed-up techniques. This very general model, which is describing most available phase based ToF systems is extended in section 3 to model a specific technique of suppressing background light, used by one manufacturer. We compared the model with a real ToF system in two different scenarios; the methods and results will be presented in section 4. Section 5 gives an conclusion and outlook.

2 A Physical Model

2.1 Assumptions

Because the investigation of errors occurring in ToF systems is not possible by regarding the isolated sensor, we have to model a whole ToF acquisition system, including a light source, the target response, the image acquisition and analysis. Our focus lies on the sensor and its noise sources, so we neglected questions about the appropriate camera model, the shape and position of the light source and scene-induced interferences like multi-reflections of the active illumination.

Our model does not simulate an area light source but employs a point light source instead (which was shown by [7] to be a good approximation). We assume the light source being located at exactly the same position as the sensor. The model uses maps containing information about the theoretical scene depth, its reflectivity and the distribution of interfering background light to cover the scene dependent quantities in a simple way.

2.2 Structure of the Model

A phase based ToF measuring setup is a system consisting of a modulated light source, a target which has some effect on the light and a ToF camera which generates data from the detected optical signal.

The model is separated into modules to ensure a high flexibility. In fig. 1 the structure and the information flow between the different modules is depicted,

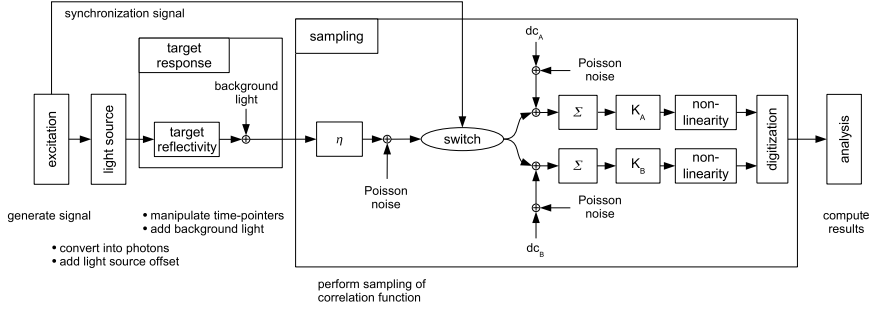


Fig. 1. Schematic representation of the model. Please see text for further information.

where a box stands for a processing unit. These units have different complexity and may consist of sub units, as it is shown for the **target response** and **sampling** module in the figure.

Excitation. The excitation module computes the function which represents the optical excitation. Furthermore a synchronization-signal is generated, which will be used in the sampling module.

Light source. Within the light source module, the excitation function is converted into a light signal. The appropriate unit of this signal is “mean number of detectable photons during one time step”, so we are working with a temporal density of photons.

Target response. The target response module simulates the response of the probe. Parameters like the target’s reflectivity are used here and the influence of additional (non-modulated) background light is taken into account. Because of the target’s distance from the light source and ToF camera, the light signal is being shifted here against the synchronization signal.

Sampling. The sampling of the correlation function at different phasings is performed in the sampling module. Incident photons generate electrons with a certain ratio η . The conversion of “mean number of present electrons” into “present electrons” is a Poisson process, so Poisson noise is added here. A switch sorts the generated electrons into the two quantum wells A and B. Now dark current electrons are added, which are also affected by Poisson noise. The sum Σ of all collected electrons of the two taps is converted into a voltage by two distinct amplification factors K_A and K_B . This voltage is transformed by a non-linear function, which simulates the effect of pixel saturation. Both resulting voltages are digitized and these digital numbers are given out.

Analysis. From the given samples of the correlation function, the output of the camera is computed here, e.g. a phase shift and an amplitude.

All modules work on a single vector which contains the signal over time. This signal can be described as a temporal density of detectable photons, but its concrete physical meaning slightly changes between the modules.

Since we want to model phenomena which are faster than one oscillating period of the light source, we have to set the temporal sampling density to a value, which is at least one hundred times higher. So for typical integration times of 10^6 oscillating periods or more for a single depth image, we get a large vector containing at least 10^8 entries.

This might be no problem for simulating a single pixel, but our goal is to model a whole ToF sensor containing up to millions of pixels, with acceptable consumption of computing time and memory. Therefore we had to seek for optimizations.

2.3 Optimizations

In order to simulate a large number of ToF pixels simultaneously it is an interesting question which of the discussed operations are pixel-dependent and which are identical for all pixels. Because of its size, the processing of the time dependent signal vector consumes a lot of computation time and memory. Therefore it is desirable to separate it into a part which is equal for all pixels and a difference term. Since the time dependent signal is affected by noise and therefore differs randomly from pixel to pixel, this is not trivial. Fortunately it can be shown that it is possible to separate the noise in an easy way:

The process of adding Poisson noise is a function which generates random numbers which are distributed according to the Poisson distribution with a parameter λ . The Poisson distribution is given by

$$P_\lambda = \frac{\lambda^k}{k!} e^{-\lambda}.$$

The parameter λ describes the mean of the values, which is here the number of generated electrons. P_λ is the probability of detecting k electrons for a given λ .

Since the Poisson distribution is reproductive, which means that

$$\begin{aligned} X_1 &\sim P_{\lambda_1} \\ X_2 &\sim P_{\lambda_2} \\ \Rightarrow X_1 + X_2 &\sim P_{\lambda_1 + \lambda_2}, \end{aligned} \tag{10}$$

several time steps collecting electrons for the same tap can be grouped, and the addition of the Poisson noise can be applied only once per group. This “grouping” is exactly what the sorting module does - so it is possible to perform the switching first, and add the Poisson noise afterwards.

Each tap experiences two Poisson processes, the electrons generated from incident photons plus a certain number of dark current electrons. Both are affected by Poisson noise and may combined in order to further speed up the simulation.

By separating the time dependent signal from its noise, we have done the critical part: All other pixel dependent operations like the multiplicative factors which describe the reflectivity of the target and the quantum efficiency of each pixel, or the additive factors like the amount of incident background light and interfering dark current electrons can simply be rearranged.

Since we now know separating the time dependent signal from its noise is allowed, it is possible to compute the switching function only once and to use these values to simulate all pixels. If the excitation function is periodical and the integration time of a subframe is an integer multiple of a oscillating period, a further speedup is achieved by computing the switching function for a single oscillating period only, and multiplying the result by the number of oscillating periods per subframe.

After rearranging the model according to that explanation, it looks as shown in fig. 2.

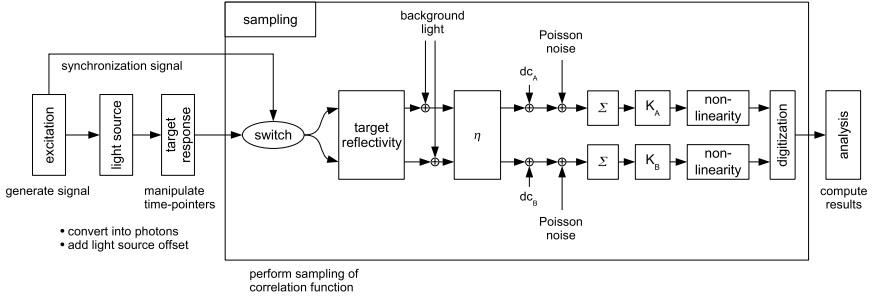


Fig. 2. Schematic representation of the model after combining Poisson processes.

By performing this sampling operation at four different phase angles $\Theta = \{0, 90, 180, 270\}^\circ$ of the input signal, we simulate the acquisition of four subframes, each consisting of two raw images. So we get eight raw images, as typically produced by a real ToF camera. Each pair of raw images corresponding to the same phasing, but different channels (one was taken by tap A, the other by tap B) are summed to decrease the influence of spatial inhomogeneities of the sensor. Now (6) is used to reconstruct a phase image, from which the depth image is being computed by using (3).

3 Suppression of Background Light

Due to its flexible structure, the model can easily be extended to describe even more complex systems. A very interesting question for developers and users of ToF systems is, how robust the system reacts to non-modulated background light. This interfering illumination causes an earlier saturation of the quantum wells, so less of the backscattered active light containing depth information is being detected, leading to a decreased signal-to-noise ratio (SNR).

So an interesting task for ToF manufacturers is to design systems which actively decrease the influence of non-modulated light. One system developed by *PMDTec* is called *Suppression of Background Illumination* (SBI), which is implemented in its *CamCube* ToF camera.

The manufacturer did not publish detailed information about the SBI, but it is possible to gather some information by analyzing the data produced by the camera.

3.1 Observations

When irradiating the cameras sensor with increasing intensities and analyzing the acquired intensity values of both channels A and B of a subframe of a certain angle Θ , the following behavior can be observed: For low intensities, there is a linear relation between the intensity of the light source and the sensors output. At some point, one of the channels gets saturated, i.e. there is almost no variation of the raw data while further increasing the intensity of the light source. At the same point, the output of the other raw-channel starts decreasing, while still increasing the irradiation level.

This behavior can be explained as follows: The charge stored in the two quantum wells Σ is continuously compared with a reference value $n_{SBI,start}$. As soon as the amount of stored charges of one quantum well exceeds this value, i.e. the difference n_{Δ} of both gets positive, a compensation process is triggered. During this process, two compensation currents are injected into the quantum wells, which contain roughly the same charge as the difference n_{Δ} . By doing that, the quantum well which contained more electrons at the beginning of the process is reset to $n_{SBI,start}$. The other quantum well is set to a value which is below its original value.

No important information is lost due to that process: The most interesting quantity which is reconstructible from the data is the phase shift φ , which gives the depth information. To estimate φ , only the difference of the two channels A and B is of importance, not their absolute value (see (6)).

3.2 Modeling SBI

These observations were included into the model (see fig. 3): The amount of charges of the two quantum wells Σ is continuously read into the SBI circuit. It computes the maximum of both and subtracts a reference value $n_{SBI,start}$ this difference is, if positive, multiplied by a factor C_{DK} , and an offset C_{D0} is added. These parameters were introduced to model eventual deviations from an ideal system.

The computed and transformed difference value is affected by Poisson noise. It is fed into two paths, which generate the compensation currents for the two quantum wells by multiplying with a factor C_{AK} (or C_{BK}) and adding an offset C_{A0} (or C_{B0}). The generated compensation currents are also affected by Poisson noise, which is regarded by the model.

By employing the property of the Poisson distribution of being reproductive (see (10)), the model can be optimized regarding the speed and memory consumption of a numerical implementation, which leads to the scheme shown in fig. 4. This model can be simulated much faster, because the SBI compensation currents are computed only once per quantum well, just before the read out

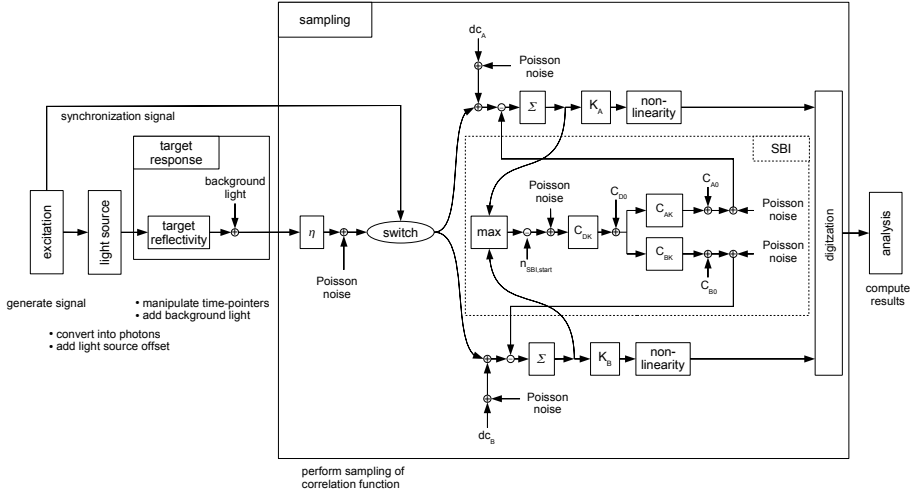


Fig. 3. Schematic representation of the model, including a SBI circuit.

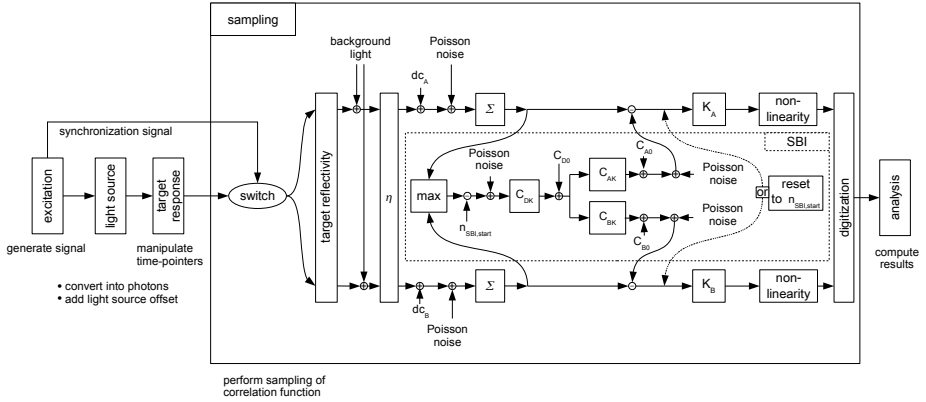


Fig. 4. Schematic representation of the model, including a SBI circuit, after combining Poisson processes.

cycle starts. In a continuous system the quantum well containing more electrons is kept on a constant level, so the additional noise caused by the SBI is canceled out by the controlling loop. We regarded that by setting the quantum well, which contained the higher number of electrons at the beginning of the SBI, to $n_{SBI,start}$ at the end of the process.

The model was implemented in *heurisko*, an image processing script language. The simulation of a ToF camera system acquiring one $1000 \times 1000 \text{ pixel}^2$ depth image, using four subframes, takes about $t = 10\text{s}$ on a Windows XP

Pentium 4 2,80GHz machine. The source code was not optimized for high speed computation yet.

4 Experimental Verification of the Model

4.1 Investigation of Noise

Method. To verify the model we used a setup similar to a radiometric calibration setup for conventional 2D cameras, as described for instance in [2]: We mounted a PMD CamCube ToF camera on an integrating sphere with a calibrated light source, so that the sensor could be illuminated homogeneously with variable intensities. The radiation energy Q was varied and we observed the mean gray value μ_y and the variance σ_y^2 of the output signal of one raw image¹.

For low intensities the camera behaves like a conventional linear camera, because the SBI is not active. By applying the *photon transfer method* we were able to determine the quantities K_A , K_B and η . The idea of this technique is to exploit the fact that the detected electrons are affected by Poisson noise, which has the property of $\mu = \sigma^2$, meaning the mean of the signal is equal the its variance. So by analyzing the relation of the known number of incident photons, the generated gray values and their variance we were able to estimate the searched parameters. Please see [2,1] for further details.

The highest observed mean gray value divided by K gave the parameter $n_{SBI,Start}$. The dark currents dc_A and dc_B and their distribution were estimated from the variance of the dark signal $\sigma_{y,0}^2$. All other non-uniformities were neglected in this simulation; especially the SBI module was set to ideal parameters.

Results of noise investigation. In fig. 5 the mean gray value minus the mean dark gray value $\mu_y - \mu_{y,0}$ and variance σ_y^2 were plotted over the radiation energy Q . Also the computed corresponding quantities as a result of the simulation were plotted in the same figure. It can be seen that model gives a good explanation for the observed data. The results of the simulation and the measured quantities are very similar in the linear range up to radiation energies of $Q = 1.7 \times 10^7$ photons/pixel. At this point the SBI is activated, which causes the sharp bend in the observed and simulated data. With increasing radiation energies the model still gives a good approximation of the real ToF camera, but starts to show slight deviations. The observed variance σ_y^2 is above the simulated quantity, which was expected, because we simulated an ideal SBI module. Note that even this ideal SBI module introduces additional noise compared to a ToF system without SBI.

4.2 Investigation of Systematic Deviations

Setup. We investigated the systematic deviations of depth data predicted by the simulation and compared them to measured data. We expected a periodical

¹ We analyzed the channel **A** of subframe I_0 , i.e. $\Theta = 0^\circ$.

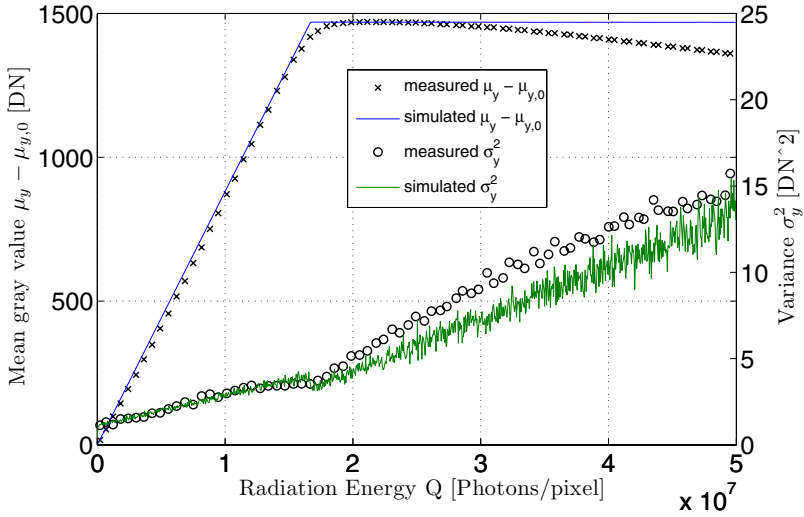


Fig. 5. Mean gray value minus mean dark gray value $\mu_y - \mu_{y,0}$ and variance σ_y^2 plotted over radiation energy Q . At $Q = 1.7 \times 10^7$ photons/pixel the SBI is activated. Please see electronic version for colors.

deviation, called “wiggling”, between the measured depth and the real depth, which is caused by higher harmonics of the optical signal. A theoretical discussion of this phenomena can be found in [11].

To determine the phase deviation of the real ToF system we mounted the camera and a plane target on movable positioning tables. The light source was demounted from the camera and attached to the target, so the targets surface was irradiated from a constant distance and the backscattered light was detected by the camera. This directly illuminated target acts like a plane emitter, which has a constant irradiance independently of its distance. So the acquired depth data does not contain deviations caused by near-field effects of the optical systems (especially the light source) nor effects caused by a varying amplitude of the optical signal.

The lengthened cable from the camera to the light source introduces an additional but constant offset of the measured phase, which can easily be corrected.

We used a telephoto lens to image only a small, homogeneously irradiated area from the middle of the target. By moving the tables to certain positions we varied the distances between the active target and the camera, and analyzed the depth data of some center pixels.

To model the periodical deviations we used a fast photo diode (Femto Photoreceiver HCA-S-400M-SI-FS) and measured the shape of the optical signal. To decrease noise, we averaged the signal over 16 oscillating periods. The measured temporal modulation of the light source is plotted in fig. 6. This real shape was

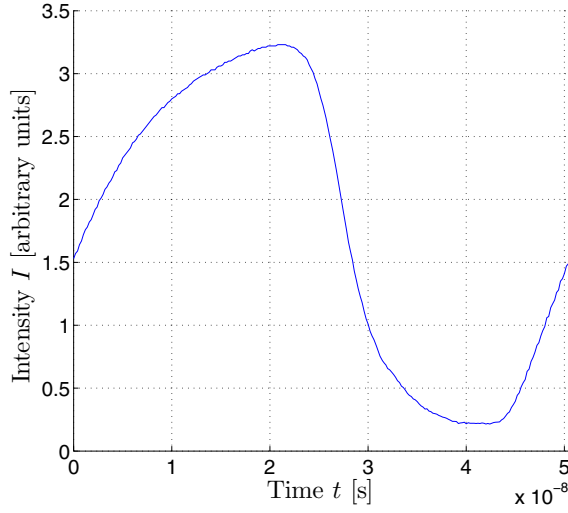


Fig. 6. Modulation of the PMD light source: intensity I plotted over time t for one oscillating period.

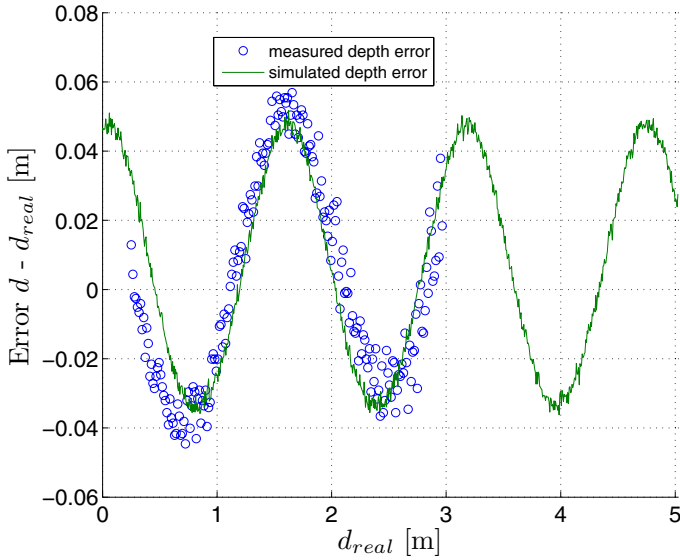


Fig. 7. Mean depth deviation of the simulated and measured distance from the real distance, plotted over the real distance.

integrated into the model and the simulation was run for a varying distance between target and camera, i.e. varying phase shifts.

Results of investigation of systematic deviations. In fig. 7 we plotted the measured and simulated depth deviations over the real depth d_{real} . The real depth can be computed from the chosen distance $d_{distance}$ between camera and target as:

$$d_{real} = 2 \cdot d_{distance} + d_{real,0}. \quad (11)$$

Note that because of the detached light source, the light has to travel the distance between target and camera only once, which explains factor 2. The distance offset $d_{real,0}$, which results from the lengthened cable and some camera internal delays of the signal, is unknown but not important for this investigation. As measured depth data we used the depth data delivered by the camera of a $10 \times 10 \text{ pixel}^2$ array near the optical axis.

The measured depth deviation has a periodical structure with a wavelength of a quarter of the ambiguity range, i.e. $7.5\text{m}/4$. Since $d_{real,0}$ is unknown, we set it to a value which fits best to the simulated data. From fig. 7 it can be seen that the model generated a very well reproduction of the measured deviation: The wavelength and amplitude of measured and simulated deviation are in very good agreement.

5 Conclusion and Outlook

We have presented a physical model of continuous-wave ToF cameras, which offers a very high flexibility. The derived simulation gives the ability to simulate data acquired by a PMD ToF sensor with low computational effort. An arbitrary optical excitation may be used to simulate the sampling of a target response by a two tap sensor, which can use any function as switching function. All spatial parameters like the reflectivity of the target seen by a single pixel, the local amount of background light or the quantum efficiency η are treated as maps and may be specified. We have integrated an additional module to the model which simulated a circuit for suppressing ambient light.

As a verification we analyzed two scenarios: The cameras response to an increasing, homogeneous irradiation as well as the systematic phase deviation caused by higher harmonics of the optical excitation. In both scenarios the model gave a precise reproduction of the observed data.

As a next step we will model *Photo response non-uniformity* (PRNU), *dark signal non-uniformity* (DSNU) and *dark current non-uniformity* (DCNU) by choosing the number of dark current electrons dc , the system gain K and the nonlinearity parameters like the fullwell capacity independently for each Gate and each pixel. We are interested in modeling also pulse-based ToF systems which will require only slight modifications of the presented model.

We see our model as an important element for the development of standards to characterize and compare Time-of-Flight systems from different manufacturers. A detailed measurement and comparison of ToF systems may be found in [1].

We are also interested in using ToF cameras for *fluorescence lifetime imaging* (FLI). By modifying the presented model, e.g. changing the input module, we will be able to simulate FLI systems.

Acknowledgment

This work is partially funded by Sony EuTec Stuttgart and the BMBF project Lynkeus. We would like to thank Michael Erz for very inspiring discussions and doing great work when acquiring the data of real ToF Systems. We also would like to thank the anonymous reviewers for giving detailed constructive and thus very useful feedback. Furthermore we would like to thank Martin Schmidt for his support with the drivers of the measurement equipment.

References

1. Erz, M., Jähne, B.: Radiometric, spectrometric and range calibrations of ToF cameras. In: Koch, R., Kolb, A. (eds.) 3rd Workshop on Dynamic 3D Imaging. LNCS, vol. 5742, pp. 16–27. Springer, Heidelberg (2009)
2. EMVA Standard 1288: EMVA Standard 1288 - Standard for Characterization of Image Sensors and Cameras. European Machine Vision Association, release 3.0, draft 1e 2009 edn. (February 2009) (to appear)
3. Elkhaili, O., Schrey, O., Ulfig, W., Brockherde, W., Hosticka, B.J., Mengel, P., Listl, L.: A 64x8 pixel 3-D CMOS time-of flight image sensor for car safety applications (2006)
4. Gokturk, S.B., Yalcin, H., Bamji, C.: A time-of-flight depth sensor - System description, issues and solutions, http://www.canesta.com/assets/pdf/technicalpapers/CVPR_Submission_TOF.pdf
5. Hasouneh, F., Knedlik, S., Peters, V., Loffeld, O.: PMD based mobile node position monitoring. In: Position, Location, And Navigation Symposium, pp. 569–573. IEEE Press, New York (2006)
6. Keller, M., Orthmann, J., Kolb, A., Peters, V.: A Simulation Framework for time-of-flight Sensors. In: Proc. of the Int. IEEE Symp. on Signals, Circuits & Systems (ISSCS), vol. 1, pp. 125–128 (2007)
7. Keller, M., Kolb, A.: Real-time Simulation of time-of-flight Sensors. Simulation Practice and Theory 17, 967–978 (2009)
8. Oggier, T., Lehmann, M., Kaufmann, R., Schweizer, M., Richter, M., Metzler, P., Lang, G., Lustenberger, F., Blanc, N.: An all-solid-state optical range camera for 3D real-time imaging with sub-centimeter depth resolution (2004)
9. Peters, V., Loffeld, O., Hartmann, K., Knedlik, S.: Modeling and Bistatic Simulation of a High Resolution 3D PMD-Camera. In: EUROSIM 2007 (6th EUROSIM Congress on Modelling and Simulation), Ljubljana, Slovenia (2007)
10. Plaue, M.: Analysis of the PMD imaging system: Technical report, Interdisciplinary Center for Scientific Computing (IWR), University of Heidelberg (2006)
11. Rapp, H.: Experimental and Theoretical Investigation of Correlating TOF-Camera Systems. Diploma thesis, Interdisciplinary Center for Scientific Computing(IWR), University of Heidelberg (2007)

12. Ringbeck, T., Hagebeuker, B.: A 3D time-of-flight camera for object detection (2007)
13. Schmidt, M.: Spatiotemporal Analysis of Range Imagery. Dissertation, IWR, Fakultät für Physik und Astronomie, University of Heidelberg (2008)
14. Schwarte, R., Heinol, H.G., Xu, Z., Hartmann, K.: New active 3D vision system based on rf-modulation interferometry of incoherent light. In: Casasent, D.P. (ed.) Society of Photo-Optical Instrumentation Engineers (SPIE) Conference Series, vol. 2588, pp. 126–134 (1995)
15. Spirig, T., Seitz, P., Heitger, F.: The lock-in CCD. Two-dimensional synchronous detection of light. *IEEE J. Quantum Electronics* 31, 1705–1708 (1995)
16. Yahav, G., Iddan, G.J., Mandelboum, D.: 3D Imaging Camera for Gaming Application (2006),
<http://www.3dvsystems.com/technology/3D%20Camera%20for%20Gaming-1.pdf>